Original Article

SHM Structural Health Monitoring

Structural Health Monitoring
2017, Vol. 16(5) 536–550

DOI: 10.1177/1475921717722725
journals.sagepub.com/home/shm
SAGE

Active vibration-based structural health monitoring system for wind turbine blade: Demonstration on an operating Vestas V27 wind turbine

Dmitri Tcherniak[1] and Lasse L Mølgaard[2]

Abstract

This study presents a structural health monitoring system that is able to detect structural defects of wind turbine blade such as cracks, leading/trailing-edge opening, or delamination. It is shown that even small defects of at least 15 cm size can be detected remotely without stopping the wind turbine. The structural health monitoring system presented is vibration-based: mechanical energy is artificially introduced by means of an electromechanical actuator, whose plunger periodically hits the blade. The induced vibrations propagate along the blade and are picked up by accelerometers mounted along the blade. The vibrations in mid-range frequencies are utilized: this range is above the frequencies excited by blade–wind interaction, ensuring a good signal-to-noise ratio. At the same time, the corresponding wavelength is short enough to deliver required damage detection resolution and long enough to be able to propagate the entire blade length. This article demonstrates the system on a Vestas V27 wind turbine. One blade of the wind turbine was equipped with the system, and a 3.5-month monitoring campaign was conducted while the turbine was operating normally. During the campaign, a defect—a trailing-edge opening—was artificially introduced into the blade and its size was gradually increased from the original 15 to 45 cm. Using a semi-supervised learning algorithm, the system was able to detect even the smallest amount of damage while the wind turbine was operating under different weather conditions. This article provides detailed information about the instrumentation and the measurement campaign and explains the damage detection algorithm.

Keywords

Wind turbines, blade damage, actuator, accelerometers, semi-supervised learning

Introduction

Blades of modern wind turbines are designed for 20–25 years of service under severe weather conditions, and during this period, damage is unavoidable. With a high probability, a small blade defect may develop into a bigger failure, and if no countermeasures are taken, may become critical, causing catastrophic consequences. Repair of a small defect is significantly cheaper than repair of a bigger one or replacement of an entire blade. Therefore, wind turbine operator companies pay close attention to structural health monitoring (SHM) of the blades. Today, this is done by periodical visual inspections conducted every 1–2 years, but many in the industry realize that a better approach is needed. Today, many approaches are suggested, attacking the problem from very different angles:[1] alongside using more robust blade design and special surface treatments to protect the blades, they include, for example, facilitating visual monitoring by means of transportable ground-based optical systems, by drones equipped with high-resolution video cameras, using thermography and many others techniques.

[1]Brüel & Kjær Sound & Vibration Measurement A/S, Nærum, Denmark
[2]Department of Applied Mathematics and Computer Science, Technical University of Denmark, Lyngby, Denmark

Corresponding author:
Dmitri Tcherniak, Brüel & Kjær Sound & Vibration Measurement A/S, Skodsborgvej 307, 2850 Nærum, Denmark.
Email: Dmitri.Tcherniak@bksv.com

One of the most promising ways is instrumenting wind turbines with vibration sensors and monitoring the blades' integrity via permanent monitoring of their vibration.[2,3] This approach is already adopted for monitoring the mechanical components of wind turbines, such as gearbox and bearings. The main advantage of such a system is that the operator/owner is notified about the occurrence of damage almost immediately after it has happened and not after 1–2 years, when it is detected by visual inspection.

SHM via vibration monitoring may be based on different physical phenomena. One of the popular vibration-based approaches is detecting changes in modal parameters: loss of structural integrity leads to reduction of stiffness, which can be detected by monitoring modal parameters. However, this approach cannot achieve the required damage resolution since the modal parameters are not very sensitive to damage.[4] Another modal-based technique is finite element (FE) model updating.[5] It can provide more detailed information about a detected damage toward its localization and identification,[6–8] but the method is prone to numerical instability due to ill-conditioned system of equations required to be solved when updating the parameters.[9]

Another well-known vibration approach is based on guided waves:[10] a piezoelectric exciter generates stress waves, which propagate through the structure and get picked by another piezoelectric sensor. Typically, a network of active sensors (which can measure and generate vibrations) is used. Blade damage can be detected and localized by monitoring how the vibration propagates from the actuators to the sensors. The guided waves approach has much better damage resolution but requires high sensor density, since the high-frequency oscillations quickly decay with the propagation distance. Using a large number of sensors adds complexity to the SHM system and negatively influences its cost, making it less attractive for the end users.

In the study by Tcherniak and Mølgaard,[11] the authors introduced another technique (patent pending), which is similar to the guided waves technique but has inherent differences: the excitation is introduced by an electromechanical actuator, and the utilized frequency range is much lower compared to the guided waves approach. The introduced vibrations are picked by an array of accelerometers. The waves at the lower frequency (around 1 kHz) can propagate longer distances, thus the technique requires far fewer sensors. At the same time, the frequency is high enough to ensure sufficient damage detection resolution (at least 15 cm size). Structural damage changes the properties of the energy propagation between the actuator and the accelerometers; this can be detected by comparing the vibration pattern in a reference (healthy) state with the damaged state.

The important feature of the suggested approach is that it is possible not only to detect damage but also to follow its development.[11] Additionally, in previous studies,[12–14] the possibility to use the technique for damage localization was demonstrated.

In Tcherniak and Mølgaard,[11] the method was applied to an SSP34m blade (34 m long) mounted on a test rig. This study reports the results when the same technique was used on an operating wind turbine.

System implementation on Vestas V27 wind turbine

In Tcherniak and Mølgaard,[11] the authors described the experiment conducted on an SSP34m blade mounted in a test rig. Test rig facilities greatly simplified the experiment: since the blade did not move and was located indoors, it required much less effort to mount accelerometers, actuators and cabling. The experiment proved that the proposed approach performs well on a modern blade, with feasible actuator location and using a reasonable number of sensors. The system managed to detect a realistic blade fault (trailing-edge opening) and follow up on its progression. However, using the test rig, we could not evaluate the robustness of the method against noise. Indeed, when operating, the wind turbine blade is subjected to wind excitation and excitation from the hub and nacelle mechanisms, which mask the signal from the actuator. In Tcherniak and Mølgaard,[11] some artificial noise (recorded on the blades of another wind turbine in operation) was mixed with the measured signals from the actuator: we had to admit that the selected signal-to-noise ratio was very much a guess. In addition, to be able to demonstrate technical feasibility of the proposed system, it was important to do it on a real operating wind turbine.

Vestas V27 wind turbine was selected for the experiment due to its availability. The wind turbine stands in the grounds of Technical University of Denmark (DTU), Department of Wind Energy (formerly known as Risø), in Denmark, near the town of Roskilde. Vestas V27 is a relatively old wind turbine, with 27 m rotor diameter and 225 kW rated power. However, this wind turbine can be considered representative of many modern wind turbines: it is an upwind, pitch-regulated, horizontal axis wind turbine. In contrast to modern wind turbines, its blades are relatively stiff, and it has only two speed regimes: 32 and 43 r/min.

For blade excitation, the same actuator was used as for the SSP34m blade experiment (Figure 1(a)). The actuator is a simple electromechanical device: a coil is mounted on a steel base; driven by an electrical pulse, the coil "shoots" the plunger toward the structure; and

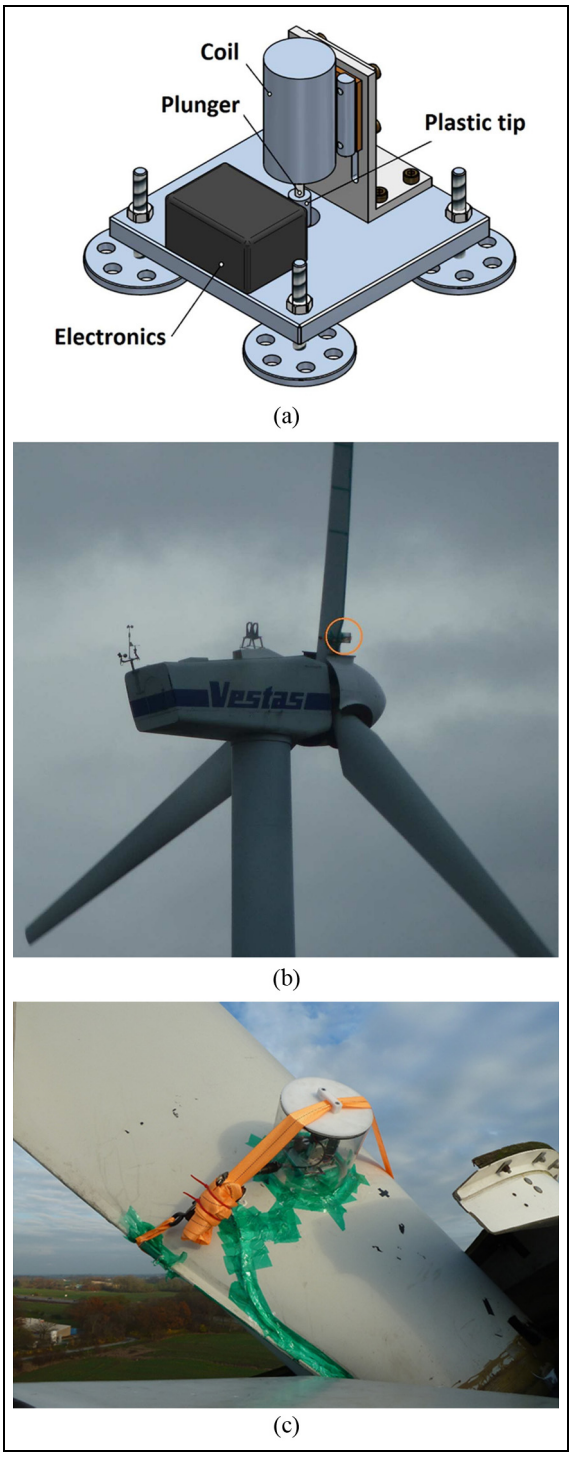

Figure 1. Actuator: (a) design, (b) actuator location inside the circle, and (c) installation on the blade.

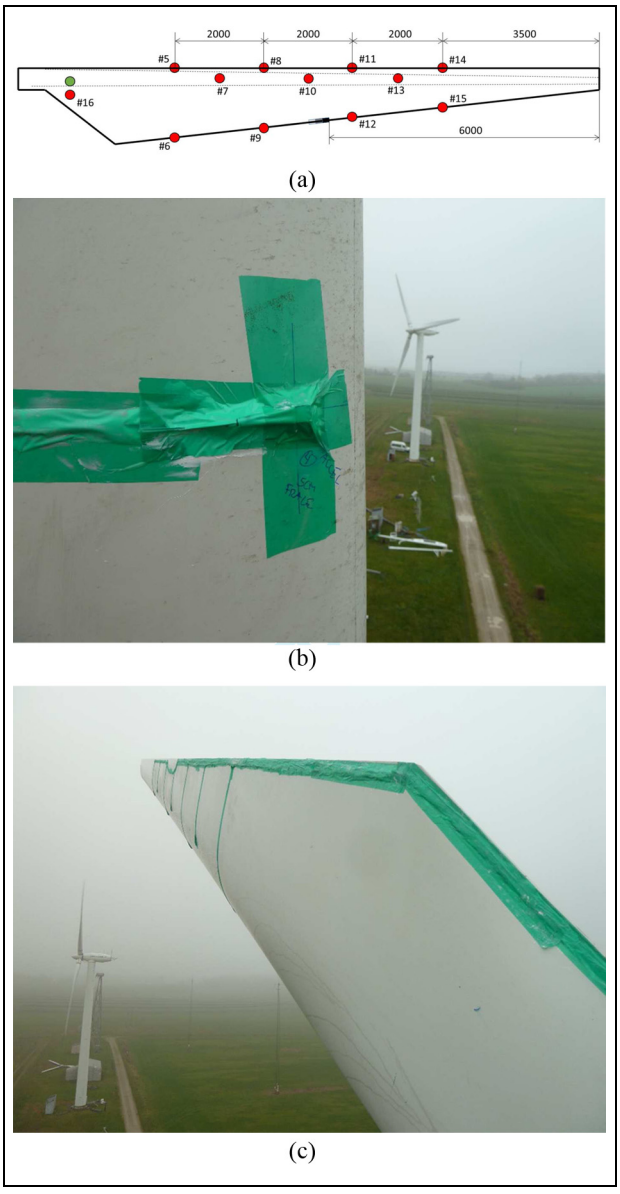

Figure 2. Blade instrumentation: (a) contour of the blade where the red circles indicate the location of the accelerometers and the green circle is the actuator position, (b) accelerometer mounted on the blade, and (c) cable arrangement.

after the hit, the plunger retracts to the initial position by means of a spring.

Due to the size of the blade, it was not possible to install the actuator inside the blade (as was done on the SSP34m blade). Instead, the actuator was installed outside the blade, on its upwind side about 1 m from the root, covered by a waterproof lid and secured with a strap (Figure 1(b) and (c)).

The vibrations were measured by accelerometers. The blade was instrumented with 12 monoaxial piezoelectric accelerometers (Brüel & Kjær Type 4507-B); their location on the blade is shown in Figure 2(a). The nominal sensitivity of accelerometers 5–15 was 10 mV/m/s^2 (Type 4507-B-004), and accelerometer 16, located near the actuator, had nominal sensitivity 1 mV/m/s^2 (Type 4507-B-001). For mounting the accelerometers,

we used plastic mounting clips, which were glued directly to the blade (no special alignment was performed, the accelerometers' measurement direction was normal to the blade surface). To protect the accelerometers, they were covered by silicon, and then, "helicopter tape" was applied on top to give the silicon a smooth shape (Figure 2(b)). The accelerometers and cables were placed on the downwind side of the blade.

The accelerometer cables run from the accelerometers toward the trailing edge and then along the trailing edge toward the blade root (Figure 2(c)). The cables were glued to the blade with silicon and covered with helicopter tape. Experience from the previous long measurement campaign on the same wind turbine[15] was used. From the same experience, we knew that such an arrangement could last several months, which is sufficient for the planned campaign, but obviously not good enough to survive on the blade for several years. For the latter case, other arrangements must be developed.

The accelerometers were connected to a data acquisition system (Brüel & Kjær Type 3660-C with two LAN-XI modules, a 12-channel input module Type 3053-B-120 and 4-channel input/output module Type 3160-A-042). Two piezoresistive direct current (DC) accelerometers Type 4574-D mounted in the spinner were used to estimate the rotor azimuth with a possibility to derive the rotational speed of the rotor. In addition, the pitch angle was measured.

The actuator was controlled by the signal from the signal generator built into one of the data acquisition modules. The generated rectangular pulse triggered the actuator's electronics, making a 100 μF capacitor discharge through the coil. Then, the capacitor was charged again to 48 V using a DC/DC converter to be ready for the next shot.

The data acquisition system and the electronics were placed in a waterproof box (dimensions $60 \times 45 \times 20$ cm^3 and weight 25 kg), which was mounted to the inner surface of the spinner (Figure 3). The equipment was powered by 24 V from the nacelle via a slip ring.

The measured data (in total, 16 signals were sampled with 16,384 Hz frequency) were wirelessly transmitted from the rotating part to the nacelle via two Cisco wireless access points, one located inside the waterproof box and another installed in the nacelle. When the turbine is operating, the line of sight between the hub and nacelle might be blocked by the steel parts of the hub. To keep an uninterrupted wireless connection, two pairs of antennas were employed: two omnidirectional antennas attached to the hub and two directional antennas mounted inside the nacelle.

The data acquisition system was controlled by Brüel & Kjær PULSE LabShop software. The software was programmed to start data acquisition, record 10 s, initiate an actuator hit and record for another 20 s. Then, acquisition was stopped and the system waited for four and a half minutes and initiated again. Thus, 12 actuator hits and corresponding datasets were produced every hour. Typical signals are shown in Figure 4.

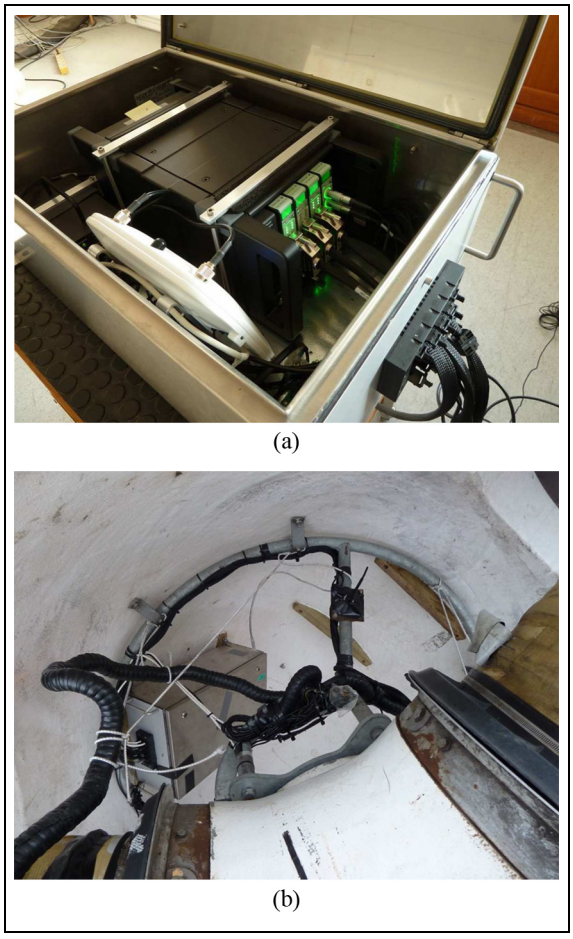

Figure 3. Data acquisition system: (a) the waterproof box with LAN-XI system (more modules are shown) and (b) the waterproof box is mounted inside the spinner but the cables are not yet connected.

Simultaneously with the vibration data, meteorological data were collected from a weather mast located a few hundred meters away. The weather data included temperature, wind speed and direction, wind turbulence at different altitudes, atmospheric pressure and precipitation; the data from the mast were delivered averaged within 1-min intervals. The power production data and yaw angle (the wind direction seen from the nacelle) were also available from the wind turbine system.

Experiment

The measurement campaign was started 28 November 2014 and finished 12 March 2015, thus lasting 104 days. With 12 actuator hits per hour (6 hits per hour during

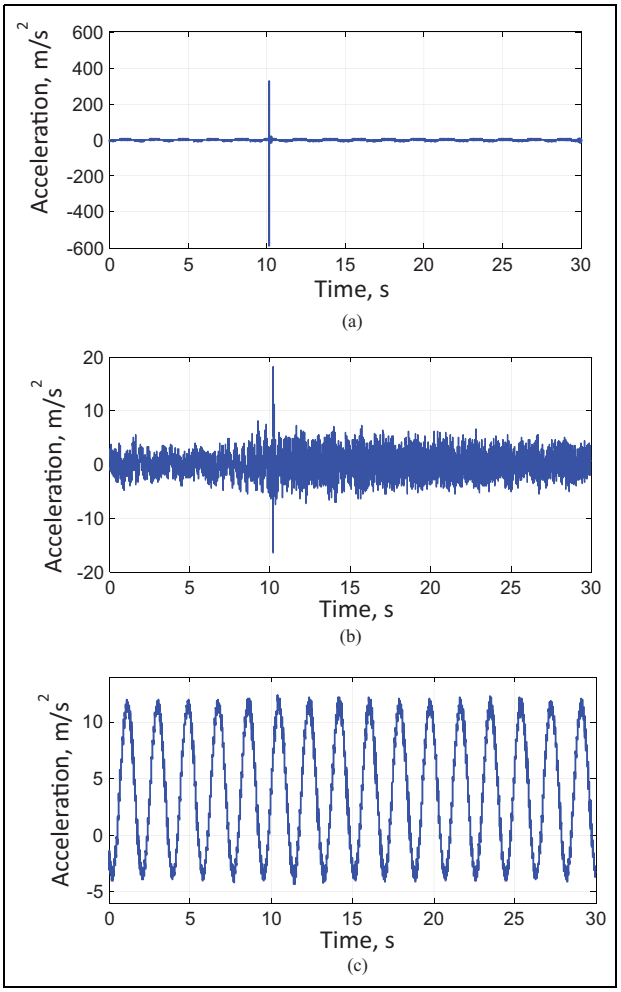

Figure 4. Typical signals: (a) accelerometer 16 (20 cm from the actuator), (b) accelerometer 15 (8.5 m from the actuator), and (c) DC accelerometer.

the Christmas and New Year eve period), data from 24,693 actuator hits were collected. During this time, the wind turbine was subjected to different weather conditions. The monitoring period covers about one-third of a year, thus no season-related events were observed. During the campaign, the turbine was in its normal power production regime, governed by its controller. However, following the agreement with the wind turbine owner, in the damaged state, we could only operate the turbine under visual surveillance, that is, during working hours. For nights, weekends and holidays, the wind turbine was set to idling (no power production), though the SHM system was kept working.

Damage implementation

For validating the capabilities of the proposed SHM system, an artificial defect was introduced in the instrumented blade. The following considerations were taken into account:

1. Input from wind turbine manufacturers and service companies regarding blades' typical defects and their location.
2. Reparability of the defect: it should be possible to repair the blade inexpensively after the end of the experiment.
3. Risk of the artificial damage developing to critical should be minimal.

In addition to this, we planned to test another property of the proposed SHM system: the indication of damage progression. For this reason, we planned to gradually increase the size of the defect.

Taken the abovementioned into account, the trailing-edge opening type of damage was selected. This is a typical defect for blades manufactured using this technology. Commercial sources, for example, Wind Energy Update,[16] inspection reports and technical papers such as Ataya and Ahmed[17] and Haselbach and Branner[18] indicate that trailing-edge failures are frequently observed in blades. Besides this, such a failure is easy to introduce, extend and repair, and according to experience, the probability that it can progress uncontrollably is very low.

The initial artificial damage was introduced on 9 December 2014 (Figure 5(a)) by technicians from service company Total Wind Group. The trailing edge was opened and extended to simulate a crack. The length of the opening was 15 cm. The opening was covered by helicopter tape to prevent atmospheric water from coming into contact with unprotected inner blade material. On 15 December 2014, the opening length was extended to 30 cm (Figure 5(b)) and 06 January 2015 to 45 cm (Figure 5(c)). On 19 January2015, the defect was repaired. The defect location in the blade is shown in Figure 2(a) and zoomed in Figure 5(d).

Data processing and damage detection

Classification

The damage detection approach used in this work is a case of anomaly or novelty detection, and the vast knowledge accumulated using this paradigm can be utilized for solving the SHM problem.[19,20] Using the terminology in the anomaly detection field, semi-supervised anomaly detection describes our approach. A supervised approach to damage detection would require recordings of a normal (healthy) operating state as well as recordings of the blades in operation with the damage that should be detected by the system. A supervised classifier could then be trained to distinguish between the

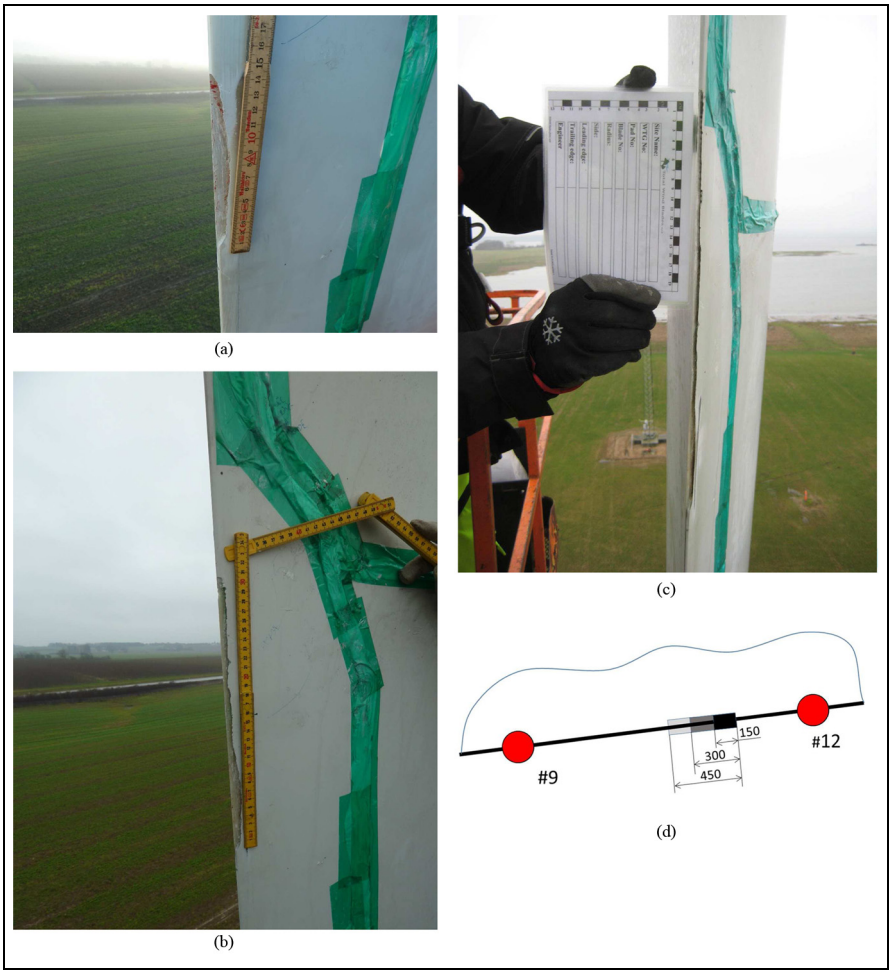

Figure 5. Implementation of the artificial blade damage. (a) Initial 15 cm trailing-edge opening, (b) extended to 30 cm, (c) extended to 45 cm, and (d) damage location in the blade relative to accelerometers and its development: 15 cm > 30 cm > 45 cm correspond to black > dark gray > light gray. The red circles are the accelerometers as in Figure 2(a).

different observed operating states. In practice, it would only be feasible to obtain operational data for a limited number of damage types, constraining the usefulness and versatility of the SHM system. Employing a semi-supervised view of the problem, we assume that only the normal (healthy) state is known, and significant deviations from this state are associated with damage. The damage detection procedure therefore includes two phases: the training phase and the detection phase. During the training phase, we assume that the structure is undamaged; here, we collect a number of samples, characterizing the normal state under different operating regimes and establish a statistical model (or models, one for every wind turbine regime) of the normal state. In the detection phase, every newly acquired sample is compared to the model of the normal state. If a significant deviation is detected, we declare that the blade is damaged.

To prepare the recordings from the accelerometers for statistical modeling, two steps must be performed: pre-processing and calculation of a feature vector. The steps are considered in the following sections.

Data processing

In the presented SHM system prototype, the data were not processed in real time (as one would expect from a commercial SHM system) but were post-processed later, when the data from several hundred actuator hits became available.

The data analysis started with processing the two DC accelerometers' signals (the example is shown in Figure 4(c)). Note that the mean of the signal is not at zero due to the centrifugal acceleration due to the rotation of the rotor. By detecting and counting the peaks, it is possible to obtain the rotations per minute and

azimuth profiles and derive the rotations per minute and azimuth values at the moment of the actuator hit.

For each actuator hit, the time history from the accelerometers, pitch angle, derived rotor rotations per minute and rotor azimuth information were combined with the weather data and saved into a database to facilitate data access.

The three main operating regimes were identified: idling, operating at 32 r/min and operating at 43 r/min. It was recognized that the vibrational data from the regimes cannot be compared directly, and further analysis was conducted separately for each regime.

Further pre-processing steps included the following:

1. Selecting the part of the signal around the actuator hit. This was done by detecting the beginning of the peak in the actuator control signal; at this step, the originally recorded 30 s of vibration data (about 500,000 time samples) are reduced to 3000 time samples per measured channel.
2. Fine alignment of the signals from different hits. This was done using the signal from accelerometer 16, closest to the actuator, since it is least affected by the noise.
3. Bandpass filtering. As mentioned in section "Introduction," a medium-frequency range (around 1 kHz) is used. The bandpass filter (BPF) was designed around this frequency (700–1200 Hz).
4. Finally, the short part of the filtered signal was extracted for the following processing: only 201 time samples between time sample 300 and 500 (inside the dashed rectangle in Figure 6(b)) was retained and used for damage feature calculation.

Figure 6 illustrates the steps of the process. It must be noted that the BPF filter parameters were found by trials, using data from the undamaged and damaged states and trying to maximize the performance of the damage detection. This approach is not feasible in the real-life scenario, where the data from the damaged blade is not available. However, based on the authors' experience gained from processing Vestas V27 and SSP34m blade data, the performance of the algorithm is only slightly affected by the fine tuning of the pre-processing parameters; using general recommendations, one can design a quite sensitive and robust SHM system. Such recommendations are design a BPF with the center frequency around 1 kHz and width 500–600 Hz and retain 200–400 time samples where all the signals attain the highest magnitude. Apparently the original design can be further improved by either testing the system mounted on a blade on a test rig or by creating "virtual test environments" based on a detailed FE model of the blade, which can simulate the acceleration responses to the actuator hits. Such "virtual environments" can be a great tool for optimizing sensors and actuator location, to tune the performance of the system toward the most realistic failures.

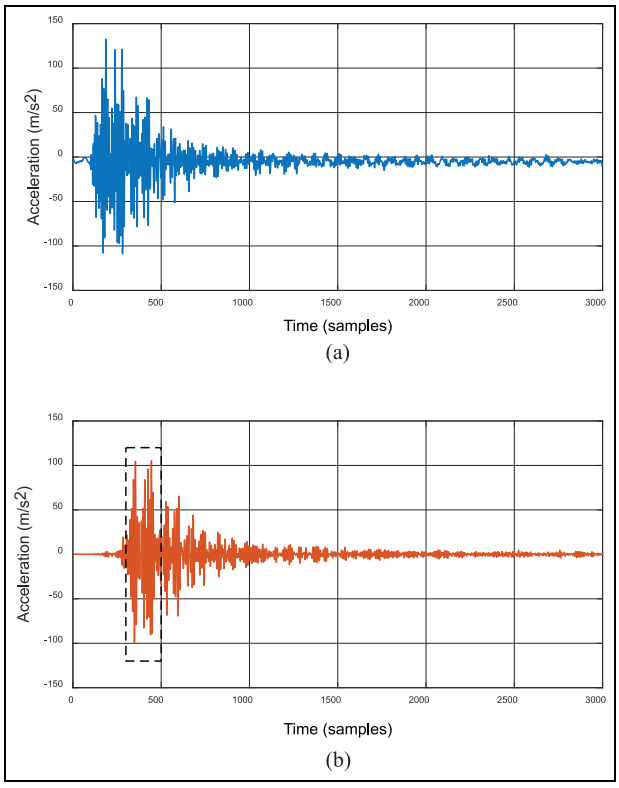

Figure 6. (a) Typical accelerometer signal (32 r/min, accelerometer 5) and (b) same signal after bandpass filtering. The dashed rectangle indicates the final trim.

Feature vector

The collection of pre-processed signals for each actuator hit must be represented using a smaller number of quantities, termed features. This representation must retain sufficient information to separate "normal" and "anomalous" operation for the subsequent statistical modeling.

Following Parker,[21] the feature vector is based on the cross-covariance between all pairs of sensor time series. Such a covariance matrix characterizes the current state of the blade. An acquired structural defect will change the energy propagation from the actuator to the sensors, which will affect the vibration pattern (relative magnitude and phase) of the measured acceleration signals. Since the cross-covariance function is a measure of similarity between two signals, the changes in the vibration pattern will be reflected as a change in the cross-covariance matrix.

For a fixed time-lag (in this study, we used zero time-lag), the covariance matrix is an $N \times N$ symmetric

matrix, where N is the number of sensors selected for the analysis (either the full set or a subset of the sensors in Figure 2(a)). The number of distinct elements in the matrix is $N(N+1)/2$. If all 12 sensors are selected, the dimensionality of the feature vector is 78. However, the values in this feature vector will exhibit multicollinearity, which will impact the subsequent fitting of a statistical model. To counter the multicollinearity, dimensionality reduction using principal component analysis (PCA) is employed. The PCA technique is a statistical method that learns a lower dimensional orthogonal representation from a set of vectors such that the extracted dimensions retain maximal variance of the data. The PCA representation of the data is learned using the covariance vectors obtained during the training phase. In this work, the number of vectors available for training is around 200 (cf. the "Results" section).

The feature vector used to represent the state of the blade for the ith actuator hit is obtained by

1. Calculating the cross-covariance matrix and reshaping it into an $N(N+1)/2$ length feature vector, which consists of the distinct elements of the cross-covariance matrix.
2. Project the feature vector into the K-dimensional PCA representation to produce the final compressed feature vector $\mathbf{x}_i$ of length K, where K is smaller than $N(N+1)/2$.

Choosing a small number of PCA dimensions to use in the subsequent modeling of the normal state can be crippling for the ability to detect damage. In this work, K was chosen such that 99% of the variance in the training data is retained.

Normal state and damage index

From each of M actuator hits obtained in the healthy state, a feature vector is extracted. The collection of M feature vectors (which is often called *training set*) are gathered to a matrix $\mathbf{X} = [\mathbf{x}_1, \mathbf{x}_2, \ldots, \mathbf{x}_M]$, $\mathbf{X} \in R^{K,M}$. This matrix forms the base for the statistical model of the healthy blade, or in other words, the normal or reference state. The feature vectors $\boldsymbol{x}_i$ are often called samples, as they reflect the state of the system at the time of the ith actuator hit. When the actuator strikes the structure and a new sample $\mathbf{y}$ arrives, the difference between the sample and the statistical model of the healthy state characterizes the health of the structure. The Mahalanobis distance is a convenient metric to quantify this difference. The Mahalanobis distance between a sample $\mathbf{y}$ and the dataset $\mathbf{X}$ is given by

$$d(y, \mathbf{X}) = \sqrt{(y - \boldsymbol{\mu}_{\mathbf{X}})^T (\Sigma_{\mathbf{X}})^{-1} (y - \boldsymbol{\mu}_{\mathbf{X}})} \tag{1}$$

where $\boldsymbol{\mu}_{\mathbf{X}} \in R^K$ is the mean of the samples in $\mathbf{X}$ and $\boldsymbol{\Sigma}_{\mathbf{X}} \in R^{K,K}$ is the covariance between the samples. This metric is selected as a *damage index* in this study. If the damage index is relatively small and does not exceed some threshold D, we declare that the system is in undamaged state. Conversely, if $d(\mathbf{y}, \mathbf{X}) > D$, we declare state $\mathbf{y}$ as damaged.

Following the semi-supervised strategy, we base the choice of the threshold D exclusively on the observations from the training phase. A naïve choice of threshold would include all points in the training set

$$D = \max_i (d(\mathbf{x}_i, \mathbf{X})) \tag{2}$$

but this choice is sensitive to outliers that could be present in the training set. Instead, we shall estimate the probability of a sample being an outlier based on the training data. The value of the threshold D can then be obtained as the $(100 - R)$th percentile of the cumulative distribution function, which means that R percent of the samples from the healthy state may exceed this value. In other words, it means that we allow R percent of false alarms in the training set, which results in a more conservative choice of the threshold. Furthermore, in this study, we use this approach to control the threshold, and R is called *allowed false alarm rate*.

In practice, all values $d_i = d(\mathbf{x}_i, \mathbf{X})$ are calculated for the selected training set $\mathbf{X}$ and sorted such that $d_j < d_{j+1}, j = 1, \ldots, M-1$. Then, the threshold D_R is selected from the sorted sequence as

$$D_R = d_k \tag{3}$$

where k is the nearest integer less than or equal to $M(100 - R)/100$.

The important feature of the damage index (1) is that (in most of the cases), its value increases with the damage development. This allows one to identify if the damage appeared but then stabilized or if it keeps progressing.

Results

As mentioned before, Vestas V27 wind turbine has a controller which operates the wind turbine in one of the three regimes:

1. Idle: the blades' pitch is about 90° so the wind turbine is not producing power. The rotor revolves due to wind shear. This regime is active if the wind is too weak (its speed is below the cut on speed).

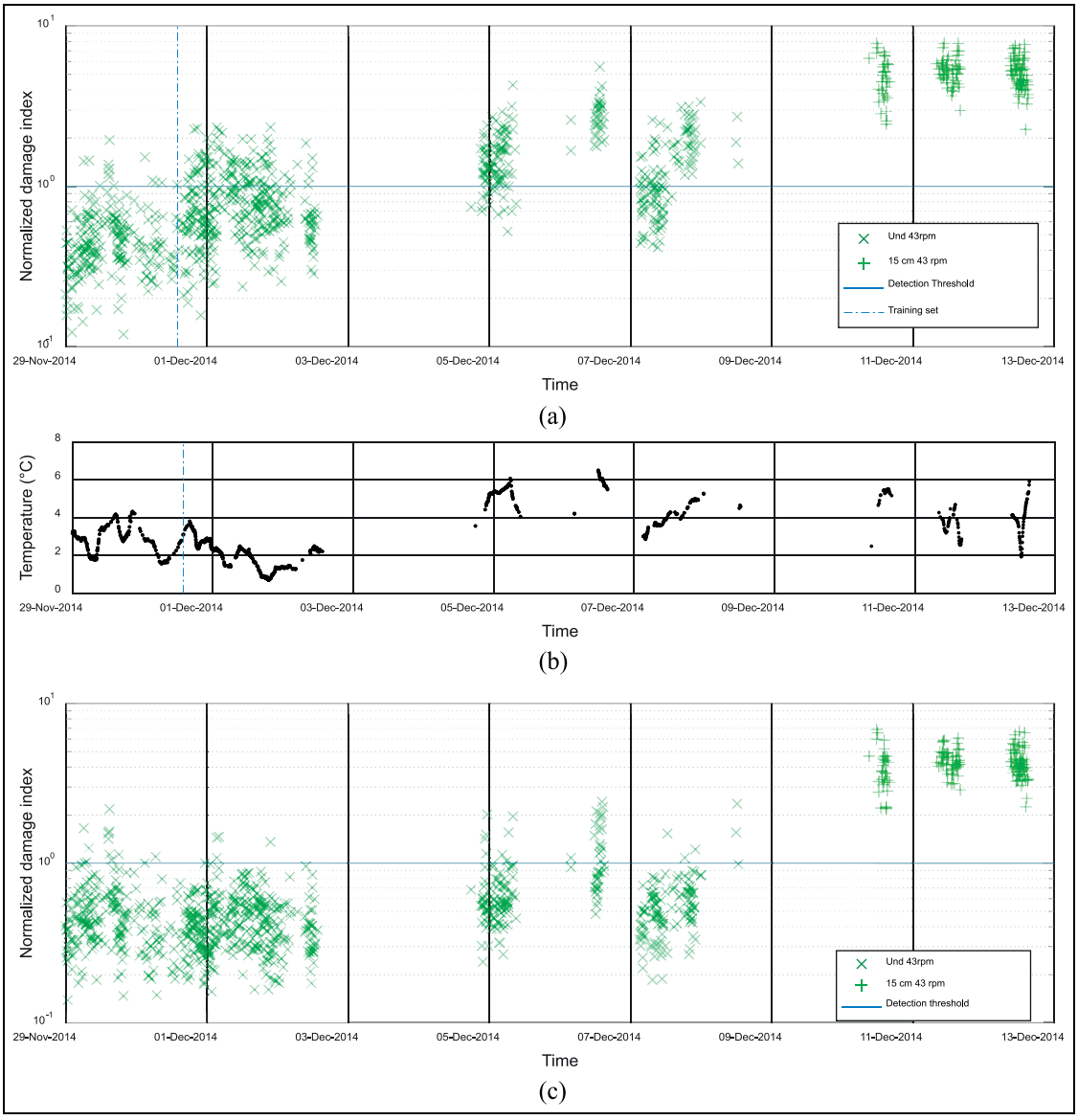

Figure 7. (a) Damage index (43 r/min regime), the training samples are picked from the beginning of the training set, left from the dash-dotted line: accepted false alarm rate 5% and test false alarm rate 48.6%. (b) Temperature when the samples were taken. (c) Damage index, the training samples are randomly picked: accepted false alarm rate 5% and test false alarm rate 8.1%.

This regime is activated if the wind turbine is broken or "switched off."

2. Low-speed production regime: the controller keeps the rotor speed constant at 32 r/min. The pitch angle for all three blades is about 0.
3. High-speed production regime: the controller keeps the rotor speed at 43 r/min. The pitch angle is about 0, though some slight variations may present.

Apparently, for SHM purposes, the latter two regimes are of the main interest: most of the time wind turbines are operating, and it is unreasonable to stop them for SHM purposes. This study addresses only the regimes when the wind turbine is operating.

Sensitivity to weather conditions

As it is well known from literature, environmental conditions influence the dynamic response of the structure and this may seriously affect the performance of an SHM algorithm. Figure 7 demonstrates this, using the data from leading- and trailing-edge accelerometers, from the 43 r/min regime. Following the scheme described in Worden and Manson,[22] the first one-third of the available 856 samples for the healthy state at

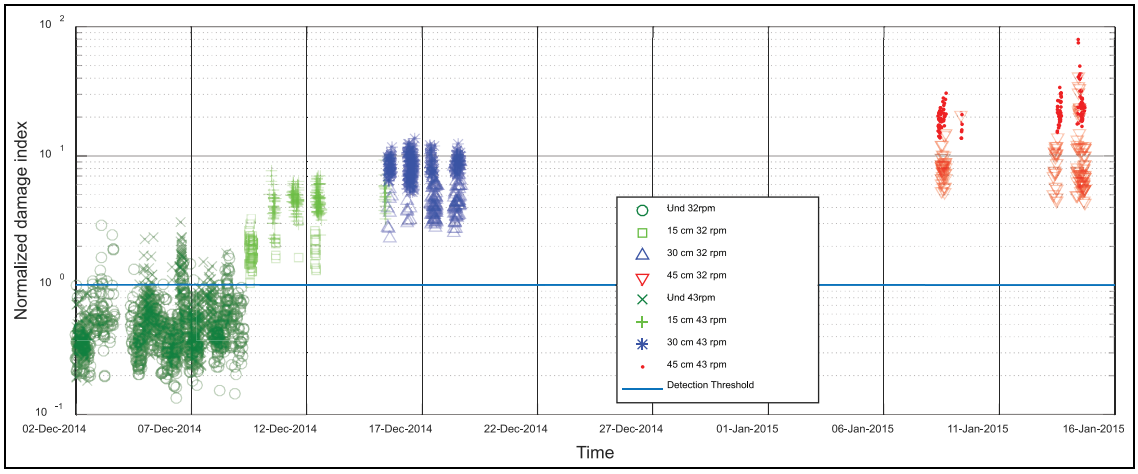

Figure 8. Damage index for all undamaged and damage cases at 32 and 43 r/min. Allowed false alarm rate is 5% and test false alarm rate is 7.3%.

43 r/min regime was used for the algorithm training. These samples are located left of the vertical dash-dotted line in Figure 7(a). Accepting 5% of false alarms in the training set ($R = 5\%$), the model of the healthy state is generated, and the threshold is found (solid horizontal line, the points below the line indicate the healthy state). The samples below the threshold line are classified as healthy state, while the samples above the threshold are declared as damaged state.

All states corresponding to the smallest amount of damage (the 15 cm crack) are identified correctly (denoted by "+"). However, validating the model against the healthy samples not included in the training set, one finds that the algorithm produces 48.6% of false alarms, which is much more than the allowed 5%. One can readily correlate the false alarms with the peaks and drops of the temperature (Figure 7(b)). Indeed, the model of the healthy state was generated when the temperature was between 2°C and 4°C, and this model fails when the temperature is outside this range.

Instead of taking the first samples, the model can be based on an equal number of samples randomly picked from the healthy state. This significantly improves the performance of the model. Figure 7(c) illustrates this for some realization of the random sequence. Now, the test false alarm rate is 8.1%, which is much closer to the allowed 5% rate.

Figure 8 demonstrates the application of this approach to *all available* data from the undamaged and damaged states, for both 32 and 43 r/min operating regimes collected during the entire monitoring period. The considered datasets contain 1684 samples for the healthy case, 224 samples for the 15 cm crack case, 310 samples for the 30 cm crack, and 237 samples for the 45 cm crack. The difference in the sample count for the different damaged states is due to the different duration of the periods, when the wind turbine was operating in these damaged states. This was due to the availability of the technicians who climbed the blade to extend the blade opening and was also dependent of the weather, when this operation was possible. The different number of samples in the damaged states does not affect the classification results, as every sample from the damaged states is considered independently. In the same way as described above, the model of the healthy state was generated based on the one-third of the available samples from the healthy state, which were randomly selected. The remaining two-third of the samples was used to validate the correctness of the healthy state classification and compute the false alarm rate.

As mentioned before, two models were used, one for each regime, and to be comparable, the damage indices d are normalized by the corresponding threshold values $D_{5\%}$. For the given random sequence, the overall false alarm rate is 7.3%, while the correct detection rate for all three crack sizes is 100%. Figure 8 also illustrates that the damage index value generally increases with the size of the crack: for the undamaged blade, the value is below 1 (for the false alarm cases, it reaches 2); for the 15 cm crack, the value is between 1 and 8; for the 30 cm crack, it is between 2 and 15; and for the 45 cm crack, it is between 4 and 80. It is not possible to make a correlation between the damage index value and the crack size (as it naturally depends on the location of damage), but one can conclude whether the crack has stabilized or continues to develop.

As mentioned before, the choice of the allowed false alarm rate R defines the detection threshold, thus affecting the resulting false alarm rate (False Positives)

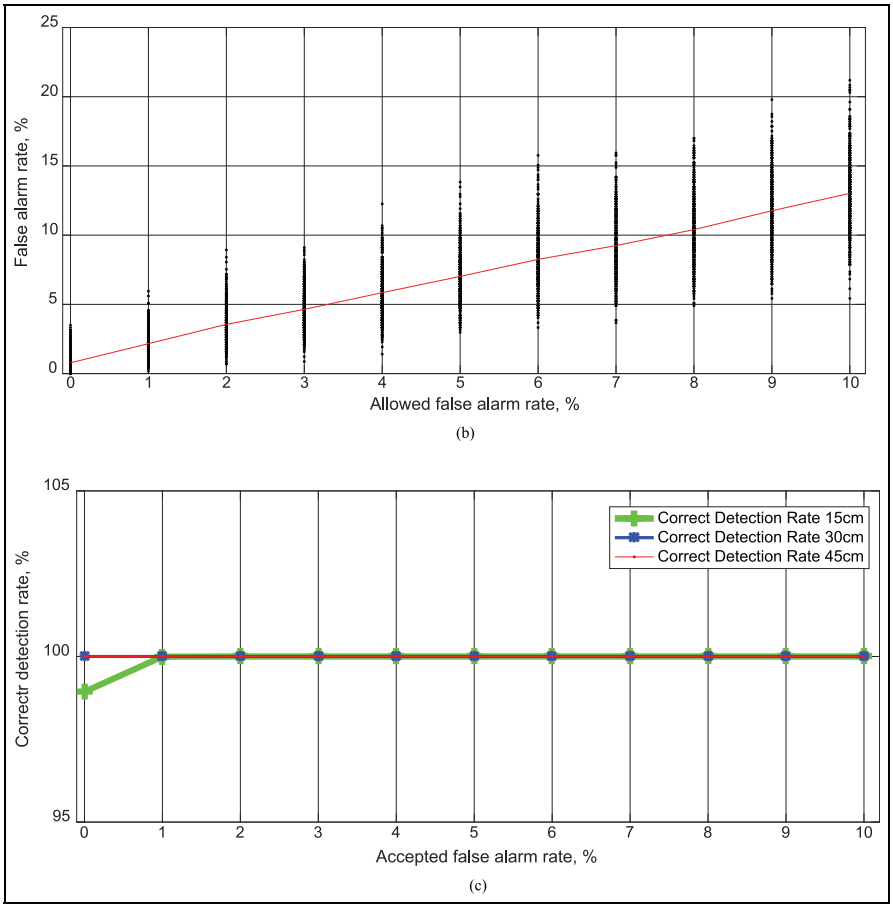

Figure 9. (a) Test false alarm rate for different allowed false alarm values for 500 random realizations of the training set and the averaged value. (b) Averaged correct detection rate for 500 realizations of the training set.

and the correct detection rate (True Positives), which in classification studies is typically illustrated by a receiver operating characteristic (ROC) curve. Here, we use a slightly different approach plotting the false alarm rate and the correct detection rate as functions of the allowed false alarm rate R (Figure 9). Since the samples of the training set are randomly selected from the healthy samples, the false alarm rate and correct detection rate depend on realization of the random sequence. Figure 9 illustrates the abovementioned: the allowed false alarm rate R was iterated from 0% to 10%; for each case, 500 random realizations of the training set were generated and the corresponding models were applied to the data. Figure 9(a) shows the development of the false alarm rate, where the dots represent the value for each random sequence realization and the line is the mean value. As expected, the mean false alarm rate is generally higher than the allowed false alarm rate; however, there exist random sequence realizations where the false alarm rate is significantly higher or significantly lower than the mean value.

Figure 9(b) shows the averaged correct detection rate. The figure is based on the data from the 43 r/min case.

Influence of different sensor configurations

The measured datasets include the data from 12 accelerometers, as shown in Figure 2. Accelerometer 16 is located close to the actuator, and its signal is only used to align time histories from the different actuator hits. Sensors 5 to 15 are distributed along the blade. In the implementation of a real SHM system, using the least number of sensors is desirable from system cost considerations. Optimization of the number of sensors and their location is out of the scope of this article; however, in this section, we provide some results of "what-if" scenarios, selecting different sensor configurations and providing the corresponding detection results and the false alarm rate.

Figure 10 compares the results for different sensor configurations computed for the 32 r/min regime. In

Figure 10(a), the results when using all 11 blade accelerometers are shown. Excluding the spar sensors (Figure 10(b)) improves the results, indicating that the spar sensors signals do not contain any information about the trailing-edge opening. Indeed, using only spar sensor for detection (Figure 10(c)) shows extremely bad detection results. It is interesting to note that using the four leading edge sensors (Figure 10(d)), the bigger amount of damage (namely, 30 and 45 cm cracks) is detectable but the algorithm fails to detect the 15 cm crack. Using the four trailing-edge sensors (Figure 10(e)), the 15 cm crack can be detected with a higher certainty; here, we observe an interesting and untypical phenomenon: the bigger amount of damage (30 cm crack) produces a smaller damage index; thus, the longer crack can be detected with the lower certainty than the bigger one.

The energy of the mechanical impact provided by the actuator propagates along the blade toward its tip; numerous reflections from the elements of the structure and blade's tip define a complex unique vibration pattern sampled by the few accelerometers. Since most of the energy propagates from the actuator toward the tip, it could be expected that a structural fault will mainly affect the readings of the accelerometers located behind the damage and, in much lesser degree, the readings of the accelerometers between the actuator and the fault. Figure 10(f) to (h) supports this suggestion: using four sensors (two on the leading edge and two on the trailing edge), the detection rate is excellent when the sensors are behind the fault (Figure 10(h)), only the 30 and 45 cm cracks are detectable when the sensors surround the fault (Figure 10(g)), and the worst results are obtained when the sensors are located between the fault and the actuator. Using this observation, it is possible to roughly locate the fault by "scanning" the blade by employing different sensor combinations.

Discussion

At 32 and 43 r/min regimes, the damage detection algorithm demonstrates comparable performance. However, in the idling case, the performance drops. It was found that this case required taking the rotor azimuth angle into account: apparently, the samples measured at different blade positions are not directly comparable. A possible reason for this is that while idling, the blade pitch is about 90° and the plunger hit direction lies in the rotor plane. Therefore, the strength of the hit is affected by gravity and depends on the azimuth angle (Figure 1(c)). When operating, the blades' pitch is around zero, the actuator direction is always perpendicular to the vector of gravity (Figure 1(b)), and the hit strength is not affected by the rotor position.

Technical implementation

As mentioned earlier, the described system is a prototype, which was implemented in order to prove the concept of an actuator-based, vibration-based SHM system. This section discusses some technical aspects of a real-life implementation of such a system.

Perhaps the most challenging part of such a system, if implemented in reality, is the accelerometers. Due to possible lightning strikes, wind turbine manufactures avoid placing any metal elements (except the components of the lightning protection system) into the blade further than one-third of its length. Apparently, the use of conventional piezoelectric accelerometers connected by copper wires is not an option for monitoring the entire blade, and they have to be replaced, for example, by metal-free optical accelerometers connected by optical fiber cables. This solution requires optical data acquisition systems. As the specifications of the currently available fiber optic, accelerometers are considerably inferior to their piezoelectric counterparts, and their performance can significantly affect the performance of the overall system, and this must be thoroughly investigated. Still, conventional piezoelectric accelerometers can be an option if only the root section of blades needs to be monitored.

Regarding the amount of data that the system has to handle, one can note it is quite moderate despite the high sampling frequency (in the described implementation, 16 kHz but can be reduced to 2–3 kHz without any effect on accuracy). Indeed, the system is not measured constantly but activated periodically, for example, once per hour (the 5-min interval used in this study is due to the need to collect a lot of data in a short period of time). The amount of data will depend on the practical implementation of the system, namely, the split of the responsibilities between the embedded system and the server. For example, if the bandpass filtering, signal alignment, calculation of the covariance matrix, and the dimensionality reduction are performed by the embedded system, then each sample is expressed by a vector of 20–30 floating-point numbers, which is up to 120 bytes. This amount of data has to be transferred to the server for classification and decision making; if the embedded system is capable of producing these steps (which involves Mahalanobis distance calculation), then the embedded system needs to transfer only few bytes to the server when damage is detected. During the training phase, it is desirable to collect the raw data (time histories), which will provide more flexibility, for example, for simple damage localization as described in previous section or if a few sensors are lost during system use.

Another crucial parameter characterizing the SHM system is its overall cost, which includes the cost of the

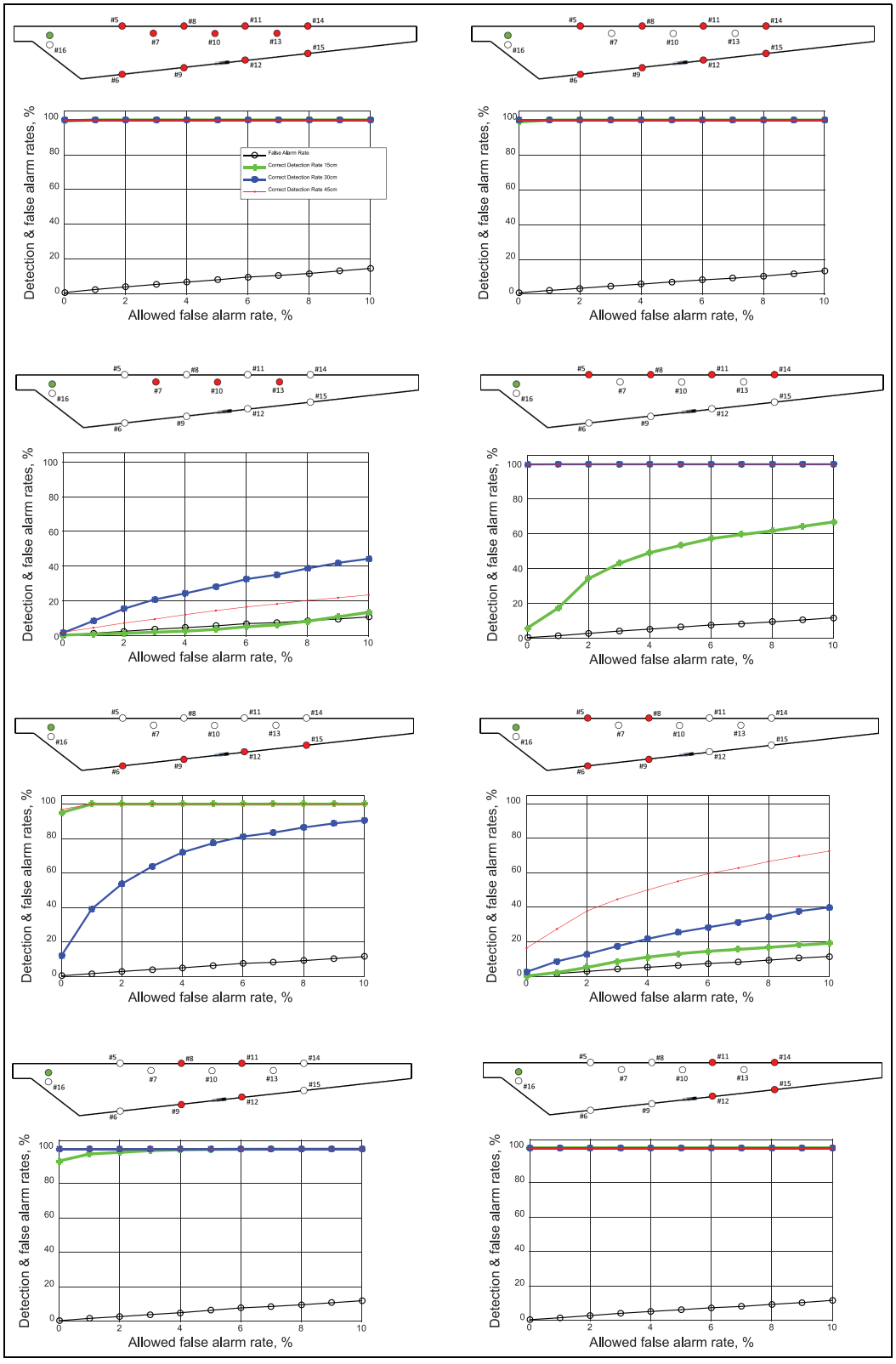

Figure 10. Test false alarm rate and correct detection rate as a function of allowed false alarm rate, for eight sensor configurations. The corresponding sensor configurations, with the engaged accelerometers shown as filled circles, are shown above the graph.

hardware, cost of installation (either retrofitting or installation during blade manufacturing), and maintenance and operational costs. The apparently high cost of such a system makes it economically feasible only for multi-megawatt wind turbines whose blades' length reaches 80–100 m. Monitoring of the full length of such a blade requires 20–30 accelerometers per blade, though the data acquisition channels can be shared between the blades using multiplexing. For long blades, a multi-actuator design (as described in Tcherniak and Mølgaard[11]), appears promising; thus, the blade can be monitored by sections. This allows a significant reduction of the data acquisition channels. Concluding, we can note that the projected cost of such a system may be considerably high; however, with a proper design, it can be notably reduced.

Conclusion and future research

This study presents an active vibration-based SHM system that utilizes an electromechanical actuator (automatic hammer) and an array of accelerometers. As a damage feature, a covariance matrix between the measured acceleration signals was used. This article describes a 3.5-month measurement campaign when the system was installed on an operating Vestas V27 wind turbine. The ability of the system to detect an artificially introduced failure (blade's trailing-edge opening) was investigated. It was demonstrated that a 15-cm-long opening can be detected without stopping the wind turbine. It can be concluded that the actuator-based approach in combination with covariance-based damage feature can be used for successful detection of typical blade defects, while using a feasible hardware setup and semi-supervised learning algorithm.

The authors see the following directions of future development. The first direction concerns creating virtual test environments, which will allow simulation of the vibration response of the blade to an actuator hit. Such environments should be based on a three-dimensional (3D) model of the blade detailed enough to realistically reproduce the time history of the acceleration responses with good resolution. The environments are a convenient tool for designing and optimizing the SHM system, as it facilitates selecting the number and location of the actuator and accelerometers, and testing the design against different types and locations of blade faults. Such a tool can also be useful to determine the minimum characteristics of the data acquisition chain. For example, using such a tool, one can evaluate the suitability of metal-free optical accelerometers in the blade SHM context.

The second direction is the improvement of the classification algorithm. First of all, the algorithm should be able to take into account the weather conditions. There are already a number of promising approaches minimizing the effect of weather conditions on the damage detection results. Another approach to improve the certainty of the classification is to utilize the sequence of observations. Indeed, the SHM system produces a binary answer (the blade is either healthy or damaged) after every actuator hit. However, there is no need to make a conclusion solely based on one observation, while many sequential observations are available. Utilizing this sequence may considerably improve the certainty of the decision making. For example, the sequential probability test ratio (SPRT) approach looks like a promising tool to benefit from the observation sequence.[23]

Acknowledgements

The authors would like to thank DTU Wind Energy for giving access to the test object.

Declaration of conflicting interests

The author(s) declared no potential conflicts of interest with respect to the research, authorship, and/or publication of this article.

Funding

This work was partly supported by EUDP (Danish Energy Technology Development and Demonstration Programme; grant number 64011-0084) Predictive Structure Health Monitoring of Wind Turbines.

References

1. Ciang CC, Lee JR and Bang HJ. Structural health monitoring for a wind turbine system: a review of damage detection methods. *Meas Sci Technol* 2008; 19(12): 122001.
2. Griffith DT, Yoder NC, Resor B, et al. Structural health and prognostics management for the enhancement of offshore wind turbine operations and maintenance strategies. *Wind Energy* 2013; 17(11): 1737–1751.
3. McGugan M, Pereira G, Sørensen BF, et al. Damage tolerance and structural monitoring for wind turbine blades. *Philos Trans A Math Phys Eng Sci* 2015; 373: 20140077.
4. Larsen GC and Berring PD. Effect of damage to modal parameters of a wind turbine blade. In: *Proceedings of the European workshop on structural health monitoring*, Nantes, 8–11 July 2014.
5. Teughels A and De Roeck G. Structural damage identification of the highway bridge Z24 by FE model updating. *J Sound Vib* 2004; 278: 589–610.
6. Ni YQ, Zhou HF, Chan KC, et al. Modal flexibility analysis of cable stayed Ting Kau bridge for damage identification. *Comput-Aided Civ Inf* 2008; 23(3): 223–236.
7. Lam HF, Yang JH and Au SK. Bayesian model updating of a coupled-slab system using field test data utilizing an

enhanced Markov chain Monte Carlo simulation algorithm. *Eng Struct* 2015; 102: 144–155.
8. Lam HF and Yang JH. Bayesian structural damage detection of steel towers using measured modal parameters. *Earthq Struct* 2015; 8(4): 935–956.
9. Hua XG, Ni YQ and Ko JM. Adaptive regularization parameter optimization in output-error-based finite element model updating. *Mech Syst Signal Pr* 2009; 23(3): 563–579.
10. Park G, Taylor GT, Farinholt KM, et al. SHM of wind turbine blades using piezoelectric active sensors. In: *Proceedings of the European workshop on structural health monitoring*, Sorento, 28 June–2 July 2010.
11. Tcherniak D and Mølgaard LL. Vibration-based SHM system: application to wind turbine blades. In: *Proceedings of the damage assessment of structures*, Ghent, 24–26 August 2015.
12. Garcia D, Tcherniak D and Trendafilova I. Damage assessment for wind turbine blades based on a multivariate statistical approach. In: *Proceedings of the international conference on damage assessment of structures*, Ghent, 24–26 August 2015.
13. Ulriksen MD, Tcherniak D and Damkilde L. Damage detection in an operating Vestas V27 wind blade by use of outlier analysis. In: *Proceedings of the IEEE workshop on environmental, energy and structural monitoring systems (EESMS)*, Trento, 9–10 July 2015. New York: IEEE.
14. Ulriksen MD, Tcherniak D, Hansen LM, et al. In-situ damage localization for a wind turbine blade through outlier analysis of SDDLV-induced stress resultants. *Struct Health Monit*. Epub ahead of print 27 December 2016. DOI: 10.1177/1475921716681727.
15. Tcherniak D and Larsen GC. Application of OMA to an operating wind turbine: now including vibration data from the blade. In: *Proceedings of the international operational modal analysis conference (IOMAC)*, Guimarães, 13–15 May 2013.
16. Wind Energy Update. *The wind energy operations & maintenance report 2016* (Wind Energy update). Industry report, 2016, http://analysis.windenergyupdate.com/
17. Ataya S and Ahmed MMZ. Damages of wind turbine blade trailing edge: forms, location, and root causes. *Eng Fail Anal* 2013; 35: 480–488.
18. Haselbach PU and Branner K. Initiation of trailing edge failure in full-scale wind turbine blade test. *Eng Fract Mech* 2016; 162: 136–154.
19. Tarassenko L, Clifton D, Bannister P, et al. Novelty detection. In: Boller C, Chang F-K and Fujino Y (eds) *Encyclopedia of structural health monitoring*. New York: John Wiley & Sons, 2009, pp. 653–675.
20. Fassois SD and Sakellariou JS. Time-series methods for fault detection and identification in vibrating structures. *Philos T Roy Soc A* 2006; 365: 411–448.
21. Parker DL. *Multi-objective design optimization framework for structural health monitoring*. PhD Thesis, Mississippi State University, Mississippi State, MS, 2011.
22. Worden K and Manson G. The application of machine learning to structural health monitoring. *Philos T R Soc A* 2007; 365: 515–537.
23. Sohn H, Allen DW, Worden K, et al. Statistical damage classification using sequential probability ratio tests. *Struct Health Monit* 2003; 2(1): 57–74.